Estimation of fractal representation of wind speed fluctuation by artificial neural network with different training algorothms

Dalibor Petković, Vlastimir Nikolić, Vojislav V. Mitić, Ljubiša Kocić

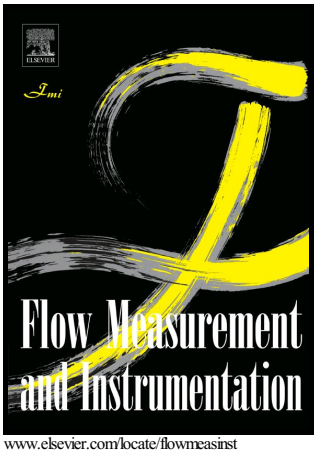

www.elsevier.com/locate/flowmeasinst

PII: S0955-5986(17)30009-2
DOI: http://dx.doi.org/10.1016/j.flowmeasinst.2017.01.007
Reference: JFMI1311

To appear in: *Flow Measurement and Instrumentation*

Received date: 23 March 2016
Revised date: 15 December 2016
Accepted date: 7 January 2017

Cite this article as: Dalibor Petković, Vlastimir Nikolić, Vojislav V. Mitić and Ljubiša Kocić, Estimation of fractal representation of wind speed fluctuation by artificial neural network with different training algorothms, *Flow Measurement and Instrumentation,* http://dx.doi.org/10.1016/j.flowmeasinst.2017.01.007

Estimation of fractal representation of wind speed fluctuation by artificial neural network with different training algorothms

Dalibor Petković[a*], Vlastimir Nikolić[b], Vojislav V. Mitić[c], Ljubiša Kocić[d]

[a]University of Niš, Pedagogical Faculty in Vranje, Partizanska 14, 17500 Vranje, Serbia
[b]University of Niš, Faculty of Mechanical Engineering, Aleksandra Medvedeva 14, 18000 Niš, Serbia
[c]Institute of Technical Sciences, Serbian Academy of Science and Art, Belgrade, Serbia
[d]University of Niš, Faculty of Electronic Engineering, Nis, Serbia

[*]corresponding author: +38164383048. dalibortc@gmail.com,

Abstract

Since the wind speed fluctuation could cause large instability in wind energy systems it is crucial to develop a method for precise estimation of the wind speed fluctuation. Fractal interpolation of the wind speed could be used to improve the accuracy of the estimation of the wind speed fluctuation. Based on the self-similarity feature, the fractal interpolation could be established from internal to external interval. In this article fractal interpolation was used to improve the wind speed fluctuation estimation by soft computing methods. Artificial neural network (ANN) with different training algorithms were used in order to estimate the wind speed fluctuation based on the fractal interpolation.

Keywords: wind speed; fractal interpolation; soft computing; prediction.

1. Introduction

Since the conventional energy sources are limited and the main reason of the world environmental pollution, there is need to increase the usage of renewable energy sources. One of the cleanest renewable energy is wind energy which becomes very popular energy sources recently. However, wind speed fluctuation is the main problem for the wind power generation since it is very randomness and uncontrollable [1].

Complex terrain could cause large fluctuation in wind speed. In other words the terrain topography could produce strongly variable wind speed [2]. There are some data-driven standardization schemes for wind speed estimation for different terrains [3]. There is large influence of the terrain on the wind speed fluctuation [4, 5]. Artificial neural networks (ANN) were applied to determine annual wind speed for some complex terrain [6]. Computational fluid dynamics (CFD) was also used for investigate the effect of the terrain features on the wind speed fluctuation [7, 8]. There is stochastic nature of the wind direction data over complex terrains [9,

10, 11]. Two-parameter Weibull probability density function was applied to model wind speed distribution but thus function cannot analyze the irregularity of the wind speed fluctuation [12].

Since wind speed fluctuation has very stochastic and unpredictably in nature, it is good to apply chaos theory based on fractal dimensions [13]. By this methodology the wind speed was modelled by the Weierstrass function with a fractal graph [14]. The wind speed series can show increment characteristic, decrement characteristic, periodical characteristic, or chaotic characteristic under different circumstance.

In this paper fractal characteristics of the wind speed fluctuation was analyzed. Detailed numerical procedure of the fractal characteristics was performed. Since the fractal characteristics were very nonlinear in nature, soft computing approach namely ANN, was applied in order to estimate the wind speed fluctuation based on the fractal characteristics. ANN model was trained with three training algorithms to investigate which algorithm could produce the best results.

2. Materials and methods

2.1. Fractals

Fractal geometry was introduced by Benoit Mandelbrot [15, 16]. Five years after, Barnsley was came with more comprehensible version of the fractal geometry [17]. Both agreed that fractals are an efficient toll for describing complex, non-Euclidean shapes. If D denotes fractal dimension, the simple inequality $D > D_T$, where D_T is topological dimension, was suggested by Mandelbrot as an acceptable definition of fractal objects.

The fractal geometry investigations were especially applied in the field of ceramics materials [18, 19]. After showing that ceramics grains surface is a fractal, the contact surface between two grains is to be understood as having much more complex geometry structure than it was thought before. The degree of knowledge concerning fractal object depends on the stride or length of the "yardstick" for measuring, i.e. $A(D) = Const \times \delta^{2/D-2}$. Figure 1 shows the relationship between the surface area A, its fractal dimension D and the stride δ.

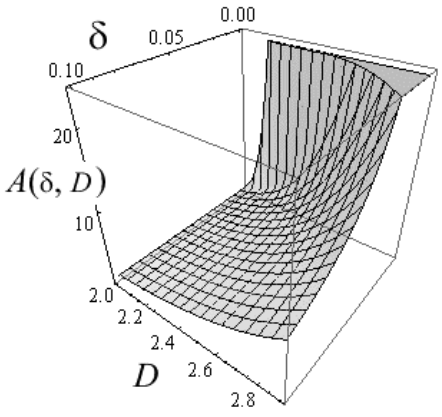

Figure 1: Size of the contact area A(δ, D) vs. fractal dimension D [20]

Such considerations helped us to estimate the capacity of one micro-contact that occurs between two neighbor ceramics grains: $C = \alpha \varepsilon_0 \varepsilon_r \frac{A(D)}{d}$ so,

$$C = \alpha \varepsilon_0 \varepsilon_r \frac{Const \times \delta^{2/D-2}}{d} = K\delta^{2/D-2}$$

From the last two formulas is clear that the surface area increases when δ gets smaller; theoretically, for $1 < DH_f$, $A \to +\infty$ when $\delta \to 0_+$. [20]

The diagram represents a graphical interpretation of dependance of the surface $A(\delta, D)$ of the fractal object on fractal dimension D and the measure unit length, which is expressed by the formula

$$A(\delta, D) = Const \times \delta^{2/D-2}$$

This formula does not depend on measuring units. It becomes clear when it multiplies by δ^{-2} which makes both sides to become dimensionless quantities, and nevertheless the diagram retains the same qualitative form.

2.2. Fractal characteristic of wind speed fluctuation

The average wind velocity in majority of cases gradually increases with height. Theoretically, on the ground level (grass, the roughness of the soil, snow layer) wind velocity it is supposed to be zero. With increasing distance from the ground, friction effect decreases and wind velocity rapidly increases and then, increment becomes slower. It does not make big difference if the atmosphere is non-stationary or stationary.

General equations of atmosphere dynamics:

$$\begin{aligned} \frac{du}{dt} &= -\frac{1}{\rho}\frac{\partial p}{\partial x} + lv, \\ \frac{dv}{dt} &= -\frac{1}{\rho}\frac{\partial p}{\partial y} - lu, \\ \frac{dw}{dt} &= -\frac{1}{\rho}\frac{\partial p}{\partial z} - g, \end{aligned} \qquad [1]$$

where $\frac{du}{dt}, \frac{dv}{dt}, \frac{dw}{dt}$ are components of air acceleration. With addition of molecular or turbulent viscosity, η (1) becomes

$$\frac{du}{dt} = -\frac{1}{\rho}\frac{\partial p}{\partial x} + 2\omega v \sin\varphi + \frac{\eta}{\rho}\left(\frac{\partial^2 u}{\partial x^2} + \frac{\partial^2 u}{\partial y^2} + \frac{\partial^2 u}{\partial z^2}\right),$$
$$\frac{dv}{dt} = -\frac{1}{\rho}\frac{d\partial}{dy} - 2\omega u \sin\varphi - 2\omega u \cos\varphi + \frac{\eta}{\rho}\left(\frac{\partial^2 u}{\partial x^2} + \frac{\partial^2 u}{\partial y^2} + \frac{\partial^2 u}{\partial z^2}\right), \quad [2]$$
$$\frac{dw}{dt} = -\frac{1}{\rho}\frac{\partial p}{\partial z} - g + 2\omega v \cos\varphi + \frac{\eta}{\rho}\left(\frac{\partial^2 w}{\partial x^2} + \frac{\partial^2 w}{\partial y^2} + \frac{\partial^2 w}{\partial z^2}\right),$$

Since the air is a continuous media, the continuity equality is to be added

$$\frac{\partial \rho}{\partial t} + \frac{\partial(\rho u)}{\partial x} + \frac{\partial(\rho v)}{\partial v} + \frac{\partial(\rho w)}{\partial z} = 0, \quad [3]$$

To complete this mathematical foundation, the equality of state

$$p = \frac{\rho R T}{\mu}, \quad [4]$$

and the adiabatic equality have to be added

$$\frac{T}{T_0} = \left(\frac{p}{p_0}\right)^{\frac{x-1}{x}}, \quad [5]$$

to get six equations with six unknown u, v, w, p, ρ, T. In the case of the heat flux dQ/dt, the (5) is replaced by

$$\frac{dT}{dt} = \frac{c_p - c_v}{c_p}\frac{T}{p}\frac{dp}{dt} + \frac{1}{c_p}\frac{T}{p}\frac{dQ}{dt} = \frac{\gamma a}{g\rho}\frac{dp}{dt} + \frac{1}{c_p}\frac{dQ}{dt}, \quad [6]$$

where $\frac{dT}{dt}$ and $\frac{dp}{dt}$ are given by

$$\frac{dT}{dt} = \frac{\partial T}{\partial t} + u\frac{\partial T}{\partial x} + v\frac{\partial T}{\partial y} + w\frac{\partial T}{\partial z},$$
$$\frac{dp}{dt} = \frac{\partial p}{\partial t} + u\frac{\partial p}{\partial x} + v\frac{\partial p}{\partial y} + w\frac{\partial p}{\partial z}, \quad [7]$$

If the wind blows horizontally in average, upon the supposition of air incompressibility ($d\rho/dt = 0$), but pressure bias $p = \bar{p} + p'$, the eq. (2) gets the form

$$\frac{du}{dt} = \frac{\partial u}{\partial t} + u\frac{\partial u}{\partial x} + v\frac{\partial u}{\partial y} + w\frac{\partial u}{\partial z} = -\frac{1}{\rho}\frac{\partial p}{\partial x} + 2\omega v \sin\varphi + \frac{\eta}{\rho}\left(\frac{\partial^2 u}{\partial x^2} + \frac{\partial^2 u}{\partial y^2} + \frac{\partial^2 u}{\partial z^2}\right), \quad [8]$$

$$\frac{dv}{dt} = \frac{\partial v}{\partial t} + u\frac{\partial v}{\partial x} + v\frac{\partial v}{\partial y} + w\frac{\partial v}{\partial z} = -\frac{1}{\rho}\frac{\partial p}{\partial y} - 2\omega v\cos\varphi - 2\omega v\sin\varphi + \frac{\eta}{\rho}\left(\frac{\partial^2 v}{\partial x^2} + \frac{\partial^2 v}{\partial y^2} + \frac{\partial^2 v}{\partial z^2}\right), \quad [9]$$

Now, the continuity equality (3) becomes

$$\frac{\partial u}{\partial x} + \frac{\partial v}{\partial y} + \frac{\partial w}{\partial z} = 0\ ,$$

which, after multiplication with *u* and added to (8) and by *v* and added to (9) yields

$$\frac{du}{dt} = \frac{\partial u}{\partial t} + \left(\frac{\partial u}{\partial x}\right)^2 + \frac{\partial (uv)}{\partial y} + w\frac{\partial (uw)}{\partial z} = -\frac{1}{\rho}\frac{\partial p}{\partial x} + 2\omega v\sin\varphi + \frac{\eta}{\rho}\left(\frac{\partial^2 u}{\partial x^2} + \frac{\partial^2 u}{\partial y^2} + \frac{\partial^2 u}{\partial z^2}\right), \quad [10]$$

and analogously for $\frac{dv}{dt}$. By averaging all terms of (10) over the fixed time interval *T*, we get

$$\frac{d\bar{u}}{dt} + \frac{\partial \overline{u^2}}{\partial t} + \frac{\partial \overline{uv}}{\partial y} + \frac{\partial \overline{uw}}{\partial z} = -\frac{1}{\rho}\frac{\partial \bar{p}}{\partial x} + 2\omega\bar{v}\sin\varphi + \left\{\left[\frac{\eta}{\rho}\frac{\partial^2 \bar{u}}{\partial x^2} - \frac{\partial}{\partial x}(\overline{u'u'})\right] + \left[\frac{\eta}{\rho}\frac{\partial^2 \bar{u}}{\partial y^2} - \frac{\partial}{\partial y}(\overline{u'v'})\right] + \left[\frac{\eta}{\rho}\frac{\partial^2 \bar{u}}{\partial z^2} - \frac{\partial}{\partial z}(\overline{u'w'})\right]\right\}, \quad [11]$$

Taking into account that $\eta\frac{\partial \bar{u}}{\partial x} = \tau_{xx}$, $\eta\frac{\partial \bar{u}}{\partial y} = \tau_{yx}$ and $\eta\frac{\partial \bar{u}}{\partial z} = \tau_{zx}$ are tangential stresses, directed along the *x*-axis, depending on molecular viscosity η and different velocities along all three coordinates *x*, *y* and *z*, it is possible to rewrite the expression in curled brackets of (11) in the form

$$\frac{1}{\rho}\left[\frac{\partial}{\partial x}\left(\tau_{xx} - \tau'_{xx}\right) + \frac{\partial}{\partial y}\left(\tau_{yx} - \tau'_{yx}\right) + \frac{\partial}{\partial z}\left(\tau_{zx} - \tau'_{zx}\right)\right],$$

where

$$\tau'_{xx} = -\rho\overline{u'u'},\ \tau'_{yx} = -\rho\overline{u'v'},\ \text{and}\ \ \tau'_{zx} = -\rho\overline{u'w'} \quad [12]$$

are known as Reynolds stresses.

Now, the equation for the component $\bar{u}$ of average movement can be written in the following form

$$\frac{d\bar{u}}{dt} = -\frac{1}{\rho}\frac{\partial \bar{p}}{\partial x} + 2\omega\sin\varphi\bar{v} + \frac{1}{\rho}\left[\frac{\partial(\tau_{xx} + \tau'_{xx})}{\partial x} + \frac{\partial(\tau_{yx} + \tau'_{yx})}{\partial y} + \frac{\partial(\tau_{zx} + \tau'_{zx})}{\partial z}\right], \quad [13]$$

According to Hinze [21] who first came forward with the hypothesis that the turbulent stress act like a viscous stress, i. e. they are directly proportional to the average velocity gradient. This means that

$$\tau'_{zx} = \eta' \frac{\partial \bar{u}}{\partial z},$$

where η' is called the coefficient of turbulent viscosity. Now, combining the last equality with (12), it holds

$$-\rho \overline{u'w'} = \eta' \frac{\partial \bar{u}}{\partial z}.$$

This transforms the term in square brackets from (13) into

$$\frac{1}{\rho} \frac{\partial \tau'_{zx}}{\partial z} = \frac{\gamma_1'}{\rho} \frac{\partial^2 \bar{u}}{\partial z^2}.$$

where γ represents the turbulent viscosity. It introduces the possibility of approximation of individual derivatives $\frac{du_m}{dt}$ and $\frac{dv_m}{dt}$

$$\frac{du_m}{dt} = -\frac{1}{\rho}\frac{\partial \bar{p}}{\partial x} + 2\omega \sin\varphi \bar{v} + \frac{\eta'}{\rho}\frac{\partial^2 \bar{u}}{\partial z^2},$$
$$\frac{dv_m}{dt} = -\frac{1}{\rho}\frac{\partial \bar{p}}{\partial y} - 2\omega \sin\varphi \bar{u} - 2\omega \cos\varphi \bar{w} + \frac{\eta'}{\rho}\frac{\partial^2 v}{\partial z^2}, \qquad [14]$$

where the molecular viscosity is neglected as a result of the inequality $\eta' >> \eta$ that holds in nature. Quantities

$$k_{xz} = -\overline{u'w'}\left(\frac{\partial \bar{u}}{\partial z}\right)^{-1}, \quad k_{yz} = -\overline{v'w'}\left(\frac{\partial \bar{v}}{\partial z}\right)^{-1} \qquad [15]$$

are coefficients of turbulence (or turbulent diffusion) having dimension cm^2/sec. In the case of anisotropic turbulence, $k_{xz} \neq k_{yz}$. If the linearization of turbulence coefficients $k = k_0 + cz$ is adopted, the last terms in (14) get the form

$$\frac{\partial}{\partial z}\frac{\eta'}{\rho}\frac{\partial \bar{u}}{\partial z} \quad \text{and} \quad \frac{\partial}{\partial z}\frac{\eta'}{\rho}\frac{\partial \bar{v}}{\partial z}.$$

In the lower atmospheric layers, tangential stresses τ'_{yx} and τ'_{zx} become dominant. In addition, the ground layer is characterized by constant values of τ'_{yx} and τ'_{zx} which means that wind direction does not change by height. The thickness *H* of this ground layer may range between 20 m and 100 m. It is anyway widespread accepted *H* = 50 m.

Turbulence may be characterized by *L* – ratio of turbulence. Propose that the stress τ depends only on vertical velocity gradient $\frac{\partial \bar{u}}{\partial z}$, on density ρ and turbulence ratio *L* i.e.

$$\tau = \rho L^2 \left(\frac{\partial \bar{u}}{\partial z} \right)^2 . \qquad [16]$$

On the other hand, it is reasonable to take $L = \kappa z$ where κ is dimensionless (**Von**) **Karman's constant**, describing the logarithmic velocity profile of a turbulent fluid flow near a boundary with a **no-slip condition**[1]. Estimations for κ vary from 0.38 to 0.41.

By analogy with (16), for turbulent atmosphere η can be replaced by $k\rho$, so that

$$\tau = k\rho \frac{\partial \bar{u}}{\partial z} .$$

Comparison with (16) gives turbulence coefficient

$$k = u_0 L = u_0 \kappa z . \qquad [17]$$

where the **friction velocity** $u_0 = \sqrt{\tau_\omega / \rho}$ represents **shear stress** term τ_ω for the fluid of density ρ, and κ is Karman's constant. Now, from (16) and (17) one deduces the wind profile differential equation combines the **mean horizontal wind velocity** $\bar{u}$ blowing on the height *z* above the surface, under near-neutral conditions and with a homogeneous distribution of obstacles,

$$\frac{\partial \bar{u}}{\partial z} = \frac{u_0}{\kappa z} .$$

Integration gives

$$\partial\bar{u} = \frac{u_0}{\kappa}\frac{\partial z}{z} \;\Rightarrow\; \int \partial\bar{u} = \frac{u_0}{\kappa}\int_{z_0}^{z}\frac{\partial z}{z} \;\Rightarrow\; \bar{u} = \frac{u_0}{\kappa}\ln z\Big|_{z_0}^{z} = \frac{u_0}{\kappa}\left(\ln z - \ln z_0\right) = \frac{u_0}{\kappa}\ln\frac{z}{z_0},$$

where z_0 is known as **roughness length** (or **roughness height**), which is the height (above the surface) where the wind has zero speed. So,

$$\bar{u}(z) = \frac{u_0}{\kappa}\ln\frac{z}{z_0}. \qquad [18]$$

The formula (18) is known as **wind profile logarithmic law**, and the roughness length for some characteristic terrains is *given* in the Table 1. It is empirically set that

$$\frac{1}{10}h \le z_0 \le \frac{1}{30}h, \qquad [19]$$

where h is the height of the obstacle to the wind. So, using (18), the wind speed v_r, on the referent height z_r, and v some other height z, one gets

$$v_r = \frac{u_0}{\kappa}\ln\frac{z_r}{z_0} \quad \text{and} \quad v = \frac{u_0}{\kappa}\ln\frac{z}{z_0},$$

wherefrom follows

$$\frac{v}{v_r} = \frac{\ln\left(z/z_0\right)}{\ln\left(z_r/z_0\right)} = \frac{\ln z - \ln z_0}{\ln z_r - \ln z_0}. \qquad [20]$$

The logarithmic law (18) can be derived from the Monin-Obukhov [22] similarity theory that is strictly applicable to steady-state horizontally homogeneous conditions in the surface layer. This theory says that statistical characteristics in flow dynamics are invariant with respect to similarity transformation $[x \;\; y]^T \to [ax \;\; ay]^T (a > 0)$ and it is valid for $z >> z_0$. In praxis the limits (19) for z_0 are used, with the constants $\lambda_1 = 1/10$ to $\lambda_2 = 1/30$. But, in more accurate setting, both λ_1 and λ_2 may vary depending on the environmental parameters, so it will be reasonable to use linear interpolation

$$z_0 = (1-\theta)\lambda_1 h + \theta\lambda_2 h, \;\; 0 \le \theta \le 1. \qquad [21]$$

On the other way, if we take into account fractality of the obstacles, the different formulas can be approached. Indeed, if an obstacle is some forest then, an intuitive image of some contains "thickness" as a first parameter. Some forests, like these in polar areas are very

sparse. On the other hand, some tropical forests are impossible to pass through. Some canopies are made of tinny leafs some has large heavy leaves, so that they absorb larger amount of energy from the wind blowing through such forest. The same is with crops, habitats, rocks, mountains etc.

In terms of, the "thickness" of the obstacle can be measured with fractal (Hausdorff) dimension H_d . The object of the average height *h*, can have fractal dimension between 2 and 3. In fact $H_d = 2$, for an ideally flat ground surface. The other extreme, $H_d = 3$ is reserved for a solid wall or hill cliff with enough horizontal dimension in direction orthogonal to the wind vector, to prevent the wind passing. In this case, we may set $\lambda_2 \to +\infty$, which implies nonlinear formula that will replace (21), and it is

$$z_0 = \frac{\lambda_1 h}{3 - H_d}\ ,\quad 2 \le H_d \le 3\ . \qquad [22]$$

Obviously, for ideally flat ground, $H_d = 2$, so that (22) yields $z_0 = \lambda_1 h$. For dense, impenetrable obstacle, $H_d = 3$, which gives

$$z_0 = \lim_{H_d \to 3} \frac{\lambda_1 h}{3 - H_d} = +\infty\ ,$$

which is equivalent as $\lambda_2 \to +\infty$.

Now, the formula (18) becomes

$$\bar{u}(z) = \frac{u_0}{\kappa} \ln \frac{z}{\lambda_1 h}(3 - H_d)\ , \qquad [23]$$

while (20) gives

$$v = v_r \frac{\ln z + \ln(3 - H_d) - \ln(\lambda_1 h)}{\ln z_r + \ln(3 - H_d) - \ln(\lambda_1 h)}\ .$$

Table 1: Terrain classification from Davenport [23] adapted by Wieringa [24] in terms of aerodynamic roughness length z_0

Terrain description	z_0 (m)
1. Open sea, Fetch at least 5 km	0.0002
2. Mud flats, snow; no vegetation, no obstacles	0.005
3. Grass (stricken), H=3cm	0.007*
4. Open flat terrain; grass, few isolated obstacles	0.03
5. Low crops; occasional large obstacles, $z/H > 20$	0.10
6. High crops; scattered obstacles, $15 < z/H < 20$	0.25
7. Parkland, bushes; numerous obstacles, $z/H \approx 10$	0.5
8. Regular large obstacle coverage (suburb, forest)	0.5-1.0
9. City centre with high- and low-rise buildings	≥ 2

*[25]

Four input parameters were selected for analysis: roughness length (roughness height): z_0, height-1: z_r, height-2: z, and wind speed at height-1: v_r. These parameters are considered influential on the wind speed at height-2.

2.3. Artificial neural network

An artificial neural network (ANN) has three main layers: input layer, output layer and hidden layer. The main core of the ANN is transfer function which maps the inputs to the output. The transfer function operates according to the learning rule. In this study two learning rules were used: back-propagation and extreme learning machine. Figure 2 shows the main structure of ANN. Table 3 shows optimal parameters for the ANN model in this study.

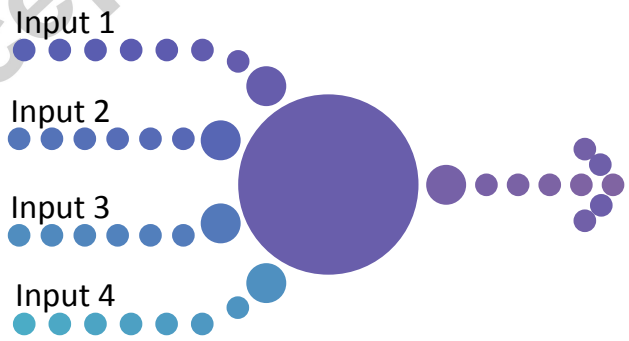

Figure 2: Structure of ANN

Table 2: Optimal parameters for the ANN modelling

ANN parameters	
Number of layers	3
Neurons	Input: 4 Hidden: 6 Output: 1
Number of iteration	10000
Activation function	Sigmoid
Learning rule 1	Back-propagation (BP)
Learning rule 2	Extreme learning machine (ELM)

Data were divided in random training and testing groups and average results were presented for all different training and testing groups in order to generalize the models' application. The average computation time for the ELM model was 380 seconds using a PC with Intel Core Duo CPU E7600 @3GHz and 4-GB RAM. The average computation time for the ANN with back propagation training algorithm using the same PC was 440 seconds. The following statistical indicators were used for the performance evaluation of models: root-mean-square error (RMSE), Pearson correlation coefficient (r) and coefficient of determination (R^2).

2. Results and discussion

Figure 3(a) presents the prediction of developed ANN model with ELM learning rule. Figure 3(b) presents the prediction of developed ANN models with BP learning rule. It can be seen that the results of the ELM learning rule is slightly better than BP learning rule according to the coefficient of determination. The number of overestimated or underestimated values produced is limited. It is obvious that the predicted values have high level of precision for the both learning rules. Table 3 summarizes the prediction accuracy results for the two models based on the three statistical indicators RMSE, r and R^2.

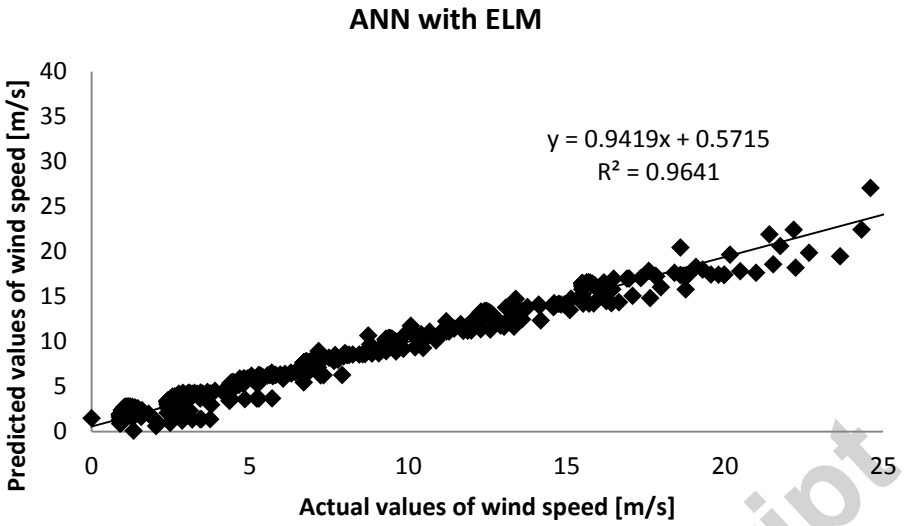

(b)

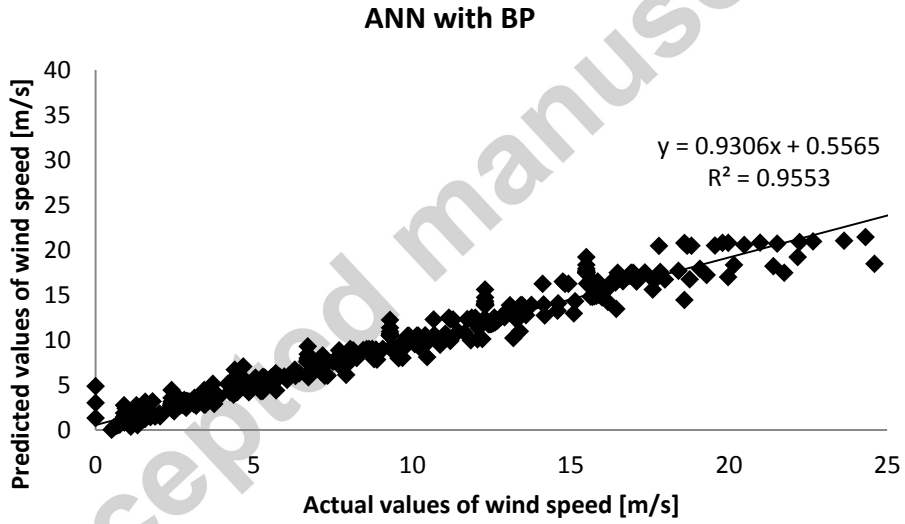

(g)

Figure 3: Wind speed fluctuation estimation by (a) ANN with ELM and (b) ANN with BP

Table 3: Performance statistics of the ELM and BP models

Learning rule	Statistical indicator		
	RMSE	R^2	r
ELM	1.1965	0.9641	0.9818
BP	1.33	0.9553	0.9774

3. Conclusion

It is crucial to develop a method for precise estimation of the wind speed fluctuation since the wind speed fluctuation could cause large instability in wind energy system. Fractal interpolation of the wind speed was used in this study to improve the accuracy of the estimation of the wind speed fluctuation. In this article fractal interpolation was used to improve the wind speed fluctuation estimation by soft computing methods. Artificial neural network (ANN) with different training algorithms were used in order to estimate the wind speed fluctuation based on the fractal interpolation. Back-propagation (BP) and extreme learning machine (ELM) were used as the learning rules of the ANN model. ELM model shown the slightly better prediction accuracy than BP model for the wind speed fluctuation estimation.

References

[1] Mitchell, S. J., Lanquaye-Opoku, N., Modzelewski, H., Shen, Y., Stull, R., Jackson, P., Ruel, J. C. (2008). Comparison of wind speeds obtained using numerical weather prediction models and topographic exposure indices for predicting windthrow in mountainous terrain. *Forest Ecology and Management*, *254*(2), 193-204.

[2] Robertson, A. (1994). Directionality, fractals and chaos in wind-shaped forests. *Agricultural and forest meteorology*, *72*(1), 133-166.

[3] He, Y. C., Chan, P. W., & Li, Q. S. (2014). Standardization of raw wind speed data under complex terrain conditions: a data-driven scheme. *Journal of Wind Engineering and Industrial Aerodynamics*, *131*, 12-30.

[4] He, Y. C., Chan, P. W., & Li, Q. S. (2013). Wind characteristics over different terrains. *Journal of Wind Engineering and Industrial Aerodynamics*, *120*, 51-69.

[5] Giovannini, L., Antonacci, G., Zardi, D., Laiti, L., & Panziera, L. (2014). Sensitivity of simulated wind speed to spatial resolution over complex terrain. *Energy Procedia*, *59*, 323-329.

[6] Lopez, P., Velo, R., & Maseda, F. (2008). Effect of direction on wind speed estimation in complex terrain using neural networks. *Renewable Energy*, *33*(10), 2266-2272.

[7] Abdi, D. S., & Bitsuamlak, G. T. (2014). Wind flow simulations on idealized and real complex terrain using various turbulence models. *Advances in Engineering Software*, *75*, 30-41.

[8] Makridis, A., & Chick, J. (2013). Validation of a CFD model of wind turbine wakes with terrain effects. *Journal of Wind Engineering and Industrial Aerodynamics*, *123*, 12-29.

[9] Sharples, J. J., McRae, R. H. D., & Weber, R. O. (2010). Wind characteristics over complex terrain with implications for bushfire risk management. *Environmental Modelling & Software*, *25*(10), 1099-1120.

[10] Lubitz, W. D., & White, B. R. (2007). Wind-tunnel and field investigation of the effect of local wind direction on speed-up over hills. *Journal of Wind Engineering and Industrial Aerodynamics*, *95*(8), 639-661.

[11] Miller, C. A., & Davenport, A. G. (1998). Guidelines for the calculation of wind speed-ups in complex terrain. *Journal of Wind Engineering and Industrial Aerodynamics*, *74*, 189-197.

[12] Calif, R., Emilion, R., & Soubdhan, T. (2011). Classification of wind speed distributions using a mixture of Dirichlet distributions. *Renewable energy*, *36*(11), 3091-3097.

[13] Serpa, C., & Buescu, J. (2015). Explicitly defined fractal interpolation functions with variable parameters. *Chaos, Solitons & Fractals*, *75*, 76-83.

[14] Xiu, C., Wang, T., Tian, M., Li, Y., & Cheng, Y. (2014). Short-term prediction method of wind speed series based on fractal interpolation. *Chaos, Solitons & Fractals*, *68*, 89-97.

[15] Fractals, M. B. L. O. (1975). Forme, Hasard et Dimension. *Paris: Flammarion*, *192*.

[16] Mandelbrot, B. B. (1983). *The fractal geometry of nature* (Vol. 173). Macmillan.

[17] Barnsley, M. F. (2014). *Fractals everywhere*. Academic press.

[18] Mitić, V. V., Kocić, L. M., Mitrović, I., & Ristić, M. M. (1997). Models of BaTiO3 Ceramics Grains Contact Surfaces. In *The 4th IUMRS International Conference in Asia OVTA Makuhari, Chiba, Japan*.

[19] Mitić, V. V., Kocić, L. M., Miljković, M., & Petković, I. (1998). Fractals and BaTiO3-ceramic microstructure analysis. In *Modern Developments and Applications in Microbeam Analysis* (pp. 365-369). Springer Vienna.

[20] Nikolić, V., Mitić, V. V., Kocić, L., & Petković, D. (2016). Wind speed parameters sensitivity analysis based on fractals and neuro-fuzzy selection technique. *Knowledge and Information Systems*, 1-11.

[21] Hinze, J. O. (1959). Turbulence: An introduction to its mechanisms and theory. *Mechanical Engineering*.

[22] Obuhov A. M., *Turbulentnost' i dinamika atmosfery*, Gidrometeoizdat 1988.

[23] Davenport, A.G., *Rationale for determining design wind velocities*, *Journal of the Structural Division*, American Society of Civil Engineers, 86, 1960, 39–68.

[24] Wieringa, J., *Representativeness of wind observations at airports*, Bulletin of the American Meteorological Society, 61, 1980, 962–971.

[25] Hrgian A.H., F*izika atmosfery*, Gidrometeoizdat 1969.

Highlights

- The fluctuation of wind speed affects energy conversion of wind energy systems.
- Fractal characteristics of the wind speed series were analyzed.
- An improved fractal interpolation to predict the wind speed series.
- Prediction of the wind speed fractal representation was established.